

1 **The effect of CO on CO₂ methanation over Ru/Al₂O₃ catalysts:**
2 ***a combined steady-state reactivity and transient DRIFT spectroscopy study***

3
4 Leonardo Falbo ^a, Carlo G. Visconti ^a, Luca Lietti ^{a*}, János Szanyi ^{b*}

5
6 ^a Department of Energy, Politecnico Di Milano, Milan, 20156, Italy

7 ^b Institute for Integrated Catalysis, Pacific Northwest National Laboratory, Richland, WA 99352, USA

8 *Corresponding authors: luca.lietti@polimi.it, janos.szanyi@pnnl.gov
9

10 **Keywords:** Methanation, Power-to-gas, Ru/Al₂O₃ catalyst, catalyst deactivation, DRIFTS-MS

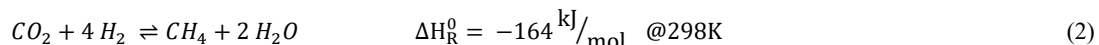
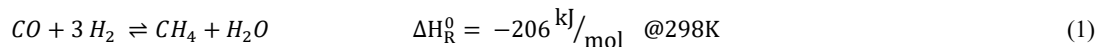
11 **Abstract**

12 The reactivity of Ru/Al₂O₃ catalysts in the hydrogenation of CO/CO₂ gas stream is investigated in this work
13 to assess the possibility of carrying out CO₂ methanation even in the presence of CO in the feed stream.
14 Such a goal is pursued by conducting reactivity studies at process conditions of industrial interest (i.e., at
15 high CO_x per-pass conversion and with concentrated CO_x/H₂ streams) and by monitoring the surface species
16 on the catalyst through transient DRIFTS-MS analysis. The catalyst shows gradual deactivation when the
17 methanation is carried out in the presence of CO in the gas feed at low temperatures (200-300 °C). However,
18 stable performance is observed at higher temperatures, showing CH₄ yields even higher than those observed
19 during methanation of a pure CO₂ feed. DRIFTS-MS experiments revealed that CO₂ methanation involves
20 a reaction pathway where CO₂ is adsorbed as bicarbonate on Al₂O₃ and successively hydrogenated to
21 methane on Ru, passing through formate and carbonyl intermediates. In the presence of CO at low
22 temperature, the catalyst shows a higher CO coverage of the Ru sites, a larger formate coverage of the
23 alumina sites and the presence of adsorbed carbonaceous species, identified as carboxylate and hydrocarbon
24 species. By carrying out the CO₂ hydrogenation on the deactivated catalyst, carboxylates remain on the
25 surface, effectively blocking CO₂ adsorption sites. However, the catalyst deactivation at low temperature is
26 reversible as thermal treatment (>350 °C) is able to restore the catalytic activity. Notably, working above
27 the carboxylate decomposition temperature ensures a clean catalyst surface, resulting in stable and high
28 performance in CO/CO₂ methanation.

1 1. Introduction

2 The growing atmospheric concentration of carbon dioxide is considered one of the main causes of global
3 warming. Accordingly, during the last 20 years, several studies were carried out for intensifying the
4 technologies aiming at its reduction [1–5]. Indeed, a drastic reduction of the CO₂ emissions to a near zero
5 or even net-negative value is required by the end of the century to keep the temperature increase lower than
6 2 °C with respect to the pre-industrial levels (*two-degree scenario* or *2DS*), which is considered a good
7 compromise to avoid dangerous climate change [6,7]. According to this scenario, carbon capture and
8 utilization (CCU) processes offer interesting perspectives. Among the suggested carbon dioxide re-
9 utilization processes, the catalytic CO₂ hydrogenation to SNG (Synthetic or Substitute Natural Gas) is very
10 attractive because it produces a fuel with a wide market and easily transportable with the existing
11 infrastructures [8–11]. In addition, when using renewable H₂ produced by water electrolysis, SNG
12 production from CO₂ hydrogenation represents a feasible route for the chemical storage of electric energy
13 produced by renewable sources/nuclear plants. In fact, considering the fluctuating and intermittent nature
14 of renewable energy sources (often collected in remote areas), an efficient way to store and to easily
15 transport this energy is desirable, instead of being wasted [12–14]. This process of long-term storage,
16 related to the use of CO₂ as carbon feedstock, is known as *Power-to-Gas* (PtG) technology [15].

17 The possibility of hydrogenating both carbon monoxide (eq.(1)) and dioxide (eq.(2)) to methane was
18 discovered at the beginning of the 20th century by Paul Sabatier [16].



21 Both reactions are strongly exothermic and bring to a molar contraction of the reacting mixture.
22 Accordingly, low temperature and high pressure boost the carbon (both CO and CO₂) conversion, as
23 reported in **Figure S1** for different CO/CO₂ ratios in the gas feed. At suitable H₂/C inlet ratio,
24 thermodynamics allows the quantitative carbon conversion even at atmospheric pressure.

25 The methanation reaction is the process of choice for the purification of H₂ derived from syngas streams,
26 but in this case the process operates with excess H₂ and diluted gas stream conditions. During the oil crisis
27 in the late '70s, methanation gained importance for the production of SNG by using syngas obtained from
28 coal gasification as feedstock [8,17]. More recently, the increase in biomass utilization led to a renewed
29 interest in the methanation reactions [12]. Regarding CO₂ methanation, the first pilot plant was built in the
30 '90s and nowadays the process is operated at commercial scale [11]. The typical feedstock is CO₂ obtained
31 by separation from biogas or from the flue gases of power plants [14,18].

32 Both CO- and CO₂-methanation reactions (eqs. (1) and (2)) are kinetically favored over VIII B group metal-
33 based supported catalysts [19]. Due to their low price [12], nickel-based catalysts are the only ones used on
34 industrial scale so far, although they are active in a temperature region where the conversion is limited by

1 thermodynamics [19]. Furthermore, Ni-based catalysts are highly subjected to carbide [20] and
2 polycarbonyl [21] formation, resulting in deactivation by sintering [22] and volatilization [12,23], as well
3 as to fouling phenomena [24] due to carbon whisker formation [20,25].

4 The most active metal for the methanation reactions is ruthenium [19,26], supported on different oxides
5 such as Al₂O₃ [27,28], TiO₂ [29,30] and CeO₂ [31,32]. Ru-based catalysts are highly stable and selective in
6 CO₂ hydrogenation, producing mostly CH₄ and only a small amount of CO as byproduct [33,34]. At the
7 same time, they are also very active in CO hydrogenation [26], producing methane and some light
8 hydrocarbons when working at low pressure and high H₂/CO molar ratio [35]. Furthermore, Ru-based
9 catalysts are less prone to deactivation than the other methanation catalysts [10], even though some
10 deactivation has been reported in the literature when working with gas feeds containing CO [36]. Sintering
11 of small Ru-particles [37,38] and formation of volatile species as Ru-carbonyls [39] are reported among the
12 possible causes of deactivation, although the most critical deactivation mechanism seems to be the
13 formation and deposition of carbonaceous species, leading to active site blocking [40]. Carbon deposition
14 is strongly affected by the process conditions [41,42] but does not lead to permanent deactivation, since
15 high temperature treatments in hydrogen can restore the initial activity [43,44]. In any case, due to their
16 high catalytic performance and long-term stability, Ru-based catalysts are attractive for process
17 intensification in SNG production from both CO and CO₂.

18 The reaction pathways operating during both CO and CO₂ hydrogenation are still debated and depend on
19 the nature of both the metal and the support, as well as on the process conditions [23,45]. On Ru-based
20 catalysts, some authors propose that CO hydrogenation involves direct dissociation of chemisorbed CO
21 (unassisted CO dissociation) [46–48], followed by a stepwise hydrogenation of adsorbed carbon to
22 methane. At variance, other authors report that CO dissociation is assisted by H₂ chemisorbed on a near-by
23 site (H-assisted CO dissociation) [45,48–50], leading to the formation of an oxygenated intermediate.
24 Concerning CO₂ methanation, most studies agree that CO is a reaction intermediate [30,51–55]. The CO
25 formation mechanism, however, is debated as well. It has been suggested that CO is produced through the
26 reverse water gas shift reaction, where the CO₂ is first adsorbed on the support surface as bicarbonate and
27 then transformed into formate species, which is the precursor of adsorbed CO on the Ru sites [54,55]. As
28 alternative route, other authors suggest that CO₂ is adsorbed dissociatively on the Ru sites, producing CO
29 and O, with the formation of some spectator species (i.e., formates) [50]. Eventually, CO is hydrogenated
30 to CH₄, according to H-assisted [48,55] or unassisted [56] pathways.

31 On these bases, the purpose of this work is to deepen the mechanistic understanding related to the CO₂
32 methanation reaction over Ru-based catalysts, with particular emphasis on the role of CO. Accordingly, the
33 hydrogenation of CO₂, CO and CO/CO₂ mixtures has been investigated. A 0.5 wt.% Ru/Al₂O₃ catalyst has
34 been considered in this study and tested in a fixed bed reactor at process conditions relevant to the industrial

1 scale SNG production. The reactivity study has been accompanied by a detailed characterization of the
2 surface species involved in both CO₂ and CO hydrogenation by using *in situ* diffuse reflectance infrared
3 Fourier-transform spectroscopy (DRIFTS).

4 2. Experimental

5 2.1. Catalysts

6 The catalyst used for the activity tests in the fixed bed reactor was a commercial 0.5 wt.% Ru/Al₂O₃ sample
7 (Aldrich, 206199). This sample, which is referred to as *Ru-SA*, came in the form of cylindrical pellets
8 ($d_p=3.2$ mm, $h_p=3.6$ mm), with eggshell geometry. The SEM-EDX analysis of an axially cut catalyst pellet
9 showed an amount of ruthenium in the external shell (thickness of 210 ± 20 μm) equal to 4.5 wt.% [33].

10 *In situ* experiments in the DRIFTS cell were carried out with a reference in-house prepared catalyst,
11 obtained by homogenous impregnation of an alumina support. Specifically, a γ -Al₂O₃ powder (Sasol
12 Puralox SCCa 150/200) was impregnated with an aqueous ruthenium nitrosyl nitrate solution (Aldrich,
13 373567) in order to obtain a nominal metal loading of 5 wt.%, a value close to the Ru amount in the
14 commercial catalyst's shell. A 30% excess of the impregnating aqueous solution with respect to the alumina
15 pore volume was used. After impregnation, the sample was dried in static air at 100 °C overnight. This
16 sample, referred to as *Ru-N*, showed comparable reactivity with respect to the commercial *Ru-SA* sample.

17 2.2. Catalyst characterization

18 Textural properties of the samples were determined by N₂ adsorption-desorption isotherms, measured at 77
19 K by using a Micromeritics Tristar 3000 instrument. Prior to the analysis, each sample was powdered and
20 evacuated at 100 °C for 3 h.

21 Transmission electron microscopy (TEM) imaging was performed on the in-house prepared catalyst (*Ru-*
22 *N*) with a high-resolution microscope (FEI Titan 80-300) operated at 300 kV, equipped with a CEOS GmbH
23 double-hexapole aberration corrector for the probe-forming lens, allowing imaging with 0.1 nm resolution.
24 The ruthenium loading of the in-house prepared supported catalyst (*Ru-N*) was determined by inductively
25 coupled plasma (ICP) mass spectrometry (Thermo Electron, X series 2 ICP-MS) on the mineralized sample,
26 successively diluted with nitric acid. The same treatment was not applicable to the commercial catalyst (*Ru-*
27 *SA*), which was not fully dissolved in the acid treatment.

28 Metal dispersion on the support was calculated by H₂ chemisorption analyses performed by a Micromeritics
29 AutoChem II instrument. The powdered catalyst (0.1 g) was loaded into a quartz reactor and activated at
30 400 °C for 3 h (2 °C/min) in a 10 vol.% H₂/Ar gas mixture at 18 L(STP)/h/g_{cat}. After activation, the sample
31 was purged in He at 400 °C for 2 h, cooled to room temperature and successively heated at 100 °C. Pulses

1 of diluted H₂ (10 vol.% H₂/Ar) were added at 100 °C and the metal dispersion was estimated based on the
2 molar ratio of adsorbed H₂ and the overall Ru loading, considering a Ru:H₂=2:1 ratio.

3 2.3. Activity tests in the macro reactor

4 Activity tests were carried out in a lab-scale rig operating 24/7 and described elsewhere in detail [33].
5 Briefly, the unit was equipped with a fixed-bed reactor (internal diameter 1.1 cm, length 23 cm), placed
6 into an electric tubular furnace. The feed gases, whose flow rate was controlled by electronic mass-flow
7 meters (Brooks Instruments), were sent to the reactor. The unconverted gases and the reaction products
8 leaving the reactor were sent to a cold trap (T=0 °C) in order to condense produced water. Reactants and
9 products were analyzed by using an on-line gas chromatograph (Agilent, 6890) equipped with two wide-
10 bore columns each connected to a thermal conductivity detector (TCD) used to quantify the concentrations
11 of H₂, Ar, N₂, CH₄, CO, CO₂ and C₂-C₅ hydrocarbons. C₃₊ hydrocarbons and oxygenated species were never
12 detected during either CO or CO₂ hydrogenation. Traces of ethane were detected only in the presence of
13 CO in the gas feed, however, its selectivity never exceeded 1% of the total carbon converted. Carbon
14 balances, defined as ratio of the total amount of carbon in the products and the converted carbon, always
15 closed within ±5%.

16 In a typical run, 0.375 g of *Ru-SA* catalyst, crushed and sieved below 106 μm, were loaded into the reactor
17 diluted with inert α-Al₂O₃ (volumetric dilution ratio equal to 1). The absence of intra- and inter-porous mass
18 transfer limitations was checked both theoretically and experimentally [33]. Prior to each run, the catalyst
19 was activated by *in situ* reduction at 400 °C (heating rate: 2 °C/min) for 3 h in pure hydrogen with a space
20 velocity of 1.8 L(STP)/h/g_{cat} and atmospheric pressure. Thereafter the reactor was cooled down to 250 °C
21 in N₂ flow (5 L(STP)/h/g_{cat}) and eventually slowly heated at 350 °C (heating rate: 1 °C/min) while the N₂
22 flow was progressively replaced by the reactant stream. The achieved process conditions (T=350 °C,
23 GHSV=5 L(STP)/h/g_{cat}, P=1 ata, H₂/CO₂=4 mol_{H2}/mol_{CO2}) were then kept until steady CO₂ conversion was
24 attained.

25 The role of CO on the catalyst activity was investigated at T=310 °C, GHSV=5 L(STP)/h/g_{cat}, P=1 ata,
26 H₂/C=4 mol_{H2}/mol_C and P⁰_{Ar}=0.01 ata, while changing the CO/CO₂ inlet ratio in the range 0-4 mol/mol
27 (**Table 1**). Reference process conditions were set at CO/CO₂=0 in **Table 1** (“CO free” conditions). The
28 effect of temperature (in the range 290-400 °C) was also investigated, while keeping constant all other
29 process conditions (GHSV=5 L(STP)/h/g_{cat}, P=1 ata, H₂/C=4 mol_{H2}/mol_C and P⁰_{Ar}=0.01 ata). The reactivity
30 of the catalyst in each run was monitored for 2 h. Long-term stability of the catalyst was also studied,
31 starting with the fresh catalyst.

1 The stability of the catalyst was evaluated by monitoring the conversion and selectivity trends with time-
 2 on-stream (T.o.S), before and after the CO co-feeding. Carbon conversion (χ_C) was calculated by using the
 3 following eq.(3):

$$4 \quad \chi_C = \frac{F_{CO_2}^{IN} + F_{CO}^{IN} - F_{CO_2}^{OUT} - F_{CO}^{OUT}}{F_{CO_2}^{IN} + F_{CO}^{IN}} \quad (3)$$

6 In eq.(3) $F_{CO_2}^{IN}$ and F_{CO}^{IN} are the inlet molar flowrates, while $F_{CO_2}^{OUT}$ and F_{CO}^{OUT} are the molar flowrates leaving
 7 the reactor, for the species CO₂ and CO, respectively.

8 **Table 1** - Gas feed compositions during the CO_x hydrogenation in the fixed bed reactor
 9 (T=310 °C, P=1 ata, GHSV=5 L(STP)/h/g_{cat}, catalyst Ru-SA)

$\frac{CO}{CO_2} \left[\frac{mol}{mol} \right]$	0	0.25	0.5	0.75	1	2	4
$\frac{CO}{CO + CO_2} \left[\frac{mol}{mol} \right]$	0	0.20	0.33	0.43	0.50	0.67	0.80
P_{CO}^0 [ata]	0	0.04	0.07	0.09	0.10	0.13	0.16
$P_{CO_2}^0$ [ata]	0.20	0.16	0.13	0.11	0.10	0.07	0.04
$P_{H_2}^0$ [ata]	0.79	0.79	0.79	0.79	0.79	0.79	0.79
P_{Ar}^0 [ata]	0.01	0.01	0.01	0.01	0.01	0.01	0.01

11 2.4. *In situ* transient DRIFTS-MS measurements

12 The *in situ* infrared spectra were collected by using a FT-IR spectrometer (ThermoFisher Nicolet iS 50R
 13 FT-IR), fitted with a liquid-N₂ cooled MCT detector and equipped with DRIFTS accessories and a high-
 14 temperature cell (Harrick, HVC-DRP). Each IR spectrum was recorded at 4 cm⁻¹ resolution and was the
 15 average of 32 scans. Collected DRIFT spectra are reported in this work as absorbance, which can be
 16 considered almost proportional to the concentration of adsorbed species on the catalyst surface [57]. The
 17 evolution of adsorbed surface species amount during the time on stream was calculated by integrating the
 18 intensity of peaks univocally related to a single adsorbed species.

19 The DRIFTS reactor cell was calibrated for a correct temperature measurement in the catalytic bed region
 20 radiated by the IR beam [58]. Two gas feeding manifolds, equipped with mass flow controllers and
 21 connected to a 4-way valve, were used to introduce gases into the reactor cell with desired flowrate and
 22 composition. The gas leaving the cell was analyzed by a mass spectrometer (UTI 100C). The following
 23 mass-to-charge ratios (m/z) were used to follow the concentration of the various species: 2 (H₂), 15 (CH₄),
 24 18 (H₂O), 28 (CO + contribution due to CO₂ fragmentation) and 44 (CO₂).

25 During the DRIFTS experiments, the undiluted Ru-N catalyst sample was placed into the reactor cell
 26 (catalyst weight around 80 mg). After activation at 350 °C for 3 h in flowing H₂ (2.4 mL/min), the catalyst
 27 was cooled down to 200 °C and purged in He for 2 h. Then H₂/He=8/92, H₂/CO₂/He=8/2/90,
 28 H₂/CO₂/He=5/5/90, H₂/CO/He=8/2/90 or H₂/CO/CO₂/He=8/1.6/0.4/90 (molar ratios) mixtures were fed

1 with a flowrate of 15 mL/min, and both the gas and the surface phase were monitored. Before each
2 experiment, the activation procedure was repeated and then a background IR spectrum in He was taken at
3 the investigated temperature.

4 3. Results and discussion

5 3.1. Catalyst characterizations

6 The commercial *Ru-SA* catalyst has an egg-shell geometry and a Ru loading in the egg-shell layer equal to
7 4.5 wt.%, measured by SEM-EDX (**Table 2**). The BET surface area of the powdered sample is 103 m²/g,
8 and the overall Ru dispersion is 35%.

9 The in-house prepared *Ru-N* catalyst has a surface area of 175 m²/g, close to that of the alumina support
10 (200 m²/g), and higher than that of the commercial material. The ruthenium loading (measured by ICP) is
11 4.4 wt.%, while the Ru-dispersion is 31%. These values are comparable to those of the eggshell *Ru-SA*
12 catalyst. The micrographs of the fresh *Ru-N* catalyst (**Figure S2**) show Ru particle sizes lower than 1 nm,
13 with a particle size distribution centered in the 6-8 Å range.

14 **Table 2** - Textural and morphological properties
15 (Metal loading: * SEM/EDX, ^x declared by producer, ⁺ ICP)

	BET surface area [m ² /g]	Metal loading [wt.%]	Metal dispersion [%]
Ru-SA	103	4.5 (shell) * 0.5 (overall) ^x	35
Ru-N	175	4.4 ⁺	31

17 3.2. Macro reactor experiments

18 As we have reported it previously [33], the *Ru-SA* catalyst exhibits stable performance during CO₂
19 methanation, with high CO₂ conversion and high carbon selectivity to methane (higher than 99% at process
20 conditions relevant for industrial scale operations, with CO being the only byproduct). The same catalyst
21 was tested in CO/CO₂ hydrogenation, keeping constant the H₂/C inlet molar ratio. The first set of CO/CO₂
22 co-feeding experiments was carried out at 310 °C by varying the CO/CO₂ ratio in the gas feed (**Table 1**).
23 **Figure 1** shows the CO₂, CO and overall C conversions as a function of time on stream (T.o.S.) for different
24 values of the CO/CO₂ ratio.

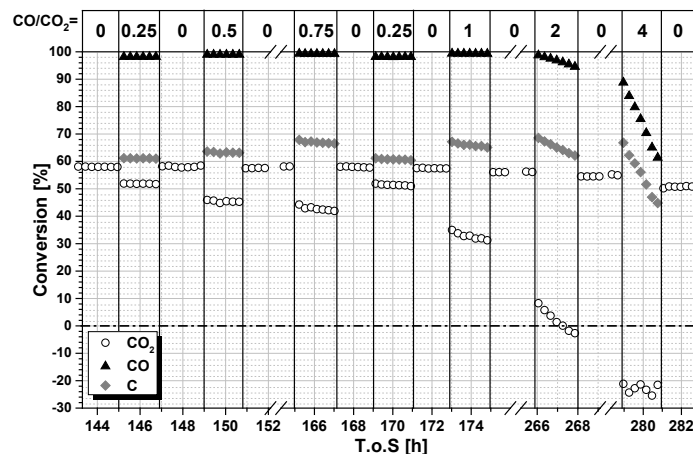
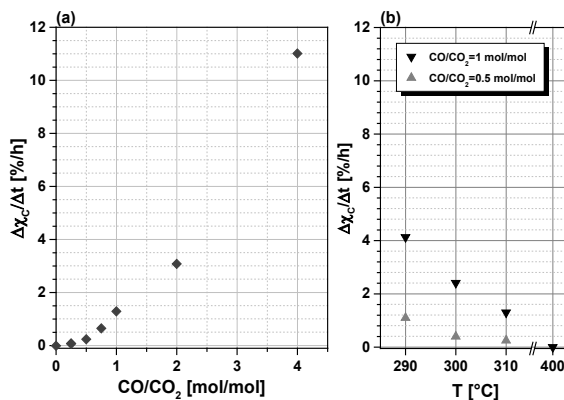


Figure 1 - Evolution with T.o.S. of CO₂, CO and CO+CO₂ (C) conversions during CO_x hydrogenation at different CO/CO₂ inlet molar ratios
 [Process conditions: T=310 °C, P=1 ata, GHSV=5 L(STP)/h/g_{cat}, H₂/C=4 mol_{H₂}/mol_C, P⁰_{Ar}=0.01 ata, catalyst: Ru-SA]

1
 2
 3
 4
 5 Under “CO free” conditions (CO/CO₂=0, T.o.S.=143-145 h in **Figure 1**) the catalyst shows a stable CO₂
 6 conversion value of 58% with a 99.5% selectivity to methane. When CO is added to the gas phase (CO/CO₂
 7 molar ratio of 0.25, T.o.S.=145-147 h) the CO₂ conversion drops to a value of 52%, while the co-fed CO is
 8 quantitatively converted. This brings to an overall C conversion higher than that measured under “CO free”
 9 conditions. Notably, the observed decrease in the CO₂ conversion is not due to a kinetic effect resulting
 10 from the decrease of P_{CO₂}, as shown in a previous kinetic study [33]. During the CO co-feeding, the process
 11 produces mainly CH₄ and only traces of ethane are detected.
 12 Experimental data indicate an inhibiting effect of CO on the CO₂ conversion, although the overall CH₄
 13 production is increased. This is in line with a scheme of consecutive reactions for the CO₂ methanation
 14 reaction, being adsorbed CO the intermediate in CH₄ formation [52]. CO admission inhibits CO₂ adsorption
 15 (thus decreasing CO₂ conversion), but pushes CH₄ formation due to CO hydrogenation. Notably, during the
 16 CO/CO₂=0.25 co-feeding period, the CO₂ conversion slightly decreases with T.o.S., showing a loss of 0.2%
 17 in 2 h on stream, while the CO conversion remains almost complete during the whole period. Returning to
 18 the “CO free” process conditions, the catalyst activity in the CO₂ hydrogenation is almost completely
 19 recovered. The process conditions with a CO/CO₂ inlet ratio of 0.25 were tested twice in order to evaluate
 20 reproducibility, which was fully confirmed (T.o.S.=169-171 h in **Figure 1**).
 21 By further increasing the CO/CO₂ inlet ratio to values of 0.5 and 0.75, the observed effects (both in terms
 22 of decrease in the CO₂ conversion and deactivation) become more pronounced; at CO/CO₂ inlet ratio equal
 23 to 1 (T.o.S.=173-175 h), besides the activity loss during the cofeeding period, the catalyst shows also an
 24 appreciable permanent deactivation when the “CO free” process conditions are restored, at T.o.S.=175 h.
 25 By further increasing the CO/CO₂ ratio to a value of 2 (T.o.S.=266 h), the CO₂ methanation inhibition due
 26 to the presence of CO in the gas feed is very strong so that CO₂ conversion suddenly drops below 10%,

1 while the CO conversion remains complete. Under these conditions, however, the catalyst is rapidly
 2 deactivated so that the CO₂ conversion at first goes to zero and then becomes even negative (i.e. CO₂
 3 becomes a reaction product). Methanation with a CO/CO₂=2 gas mixture results in a more severe catalyst
 4 deactivation and, consequently, the measured CO₂ conversion value after the CO co-feeding (T.o.S.=268
 5 h) is lower than the value measured before (T.o.S.=265 h).
 6 Deactivation effects are further amplified by working with a CO/CO₂ inlet ratio equal to 4 (T.o.S.=279-281
 7 h). As a matter of facts, the deactivation rate, calculated as loss of carbon conversion per time unit (**Figure**
 8 **2(a)**) rises more than linearly with the concentration of CO in the gas feed stream.



9
 10 **Figure 2** - Activity loss as function of (a) the CO/CO₂ inlet ratio at T=310 °C and
 11 (b) the temperature at CO/CO₂ inlet ratio equal to 0.5 and 1 molCO/molCO₂ [Other process conditions as Figure 1]

12 These results are in agreement with those described by Ekerdt and Bell [44], who reported the deactivation
 13 of Ru-based catalysts when working with H₂/CO mixtures. They showed that the deactivation rate increases
 14 with the CO partial pressure, due to an inhibition of CO on H₂ adsorption. Similar effects were also observed
 15 by other authors [40,59], although the reason for deactivation was not clearly explained. Bell et al. [60]
 16 proposed that carbon deposition was the main reason for the catalyst deactivation, while Gupta et al. [61]
 17 proposed that the formation of di- and tri-carbonyls, more difficult to hydrogenate, is responsible for the
 18 deactivation during CO hydrogenation.

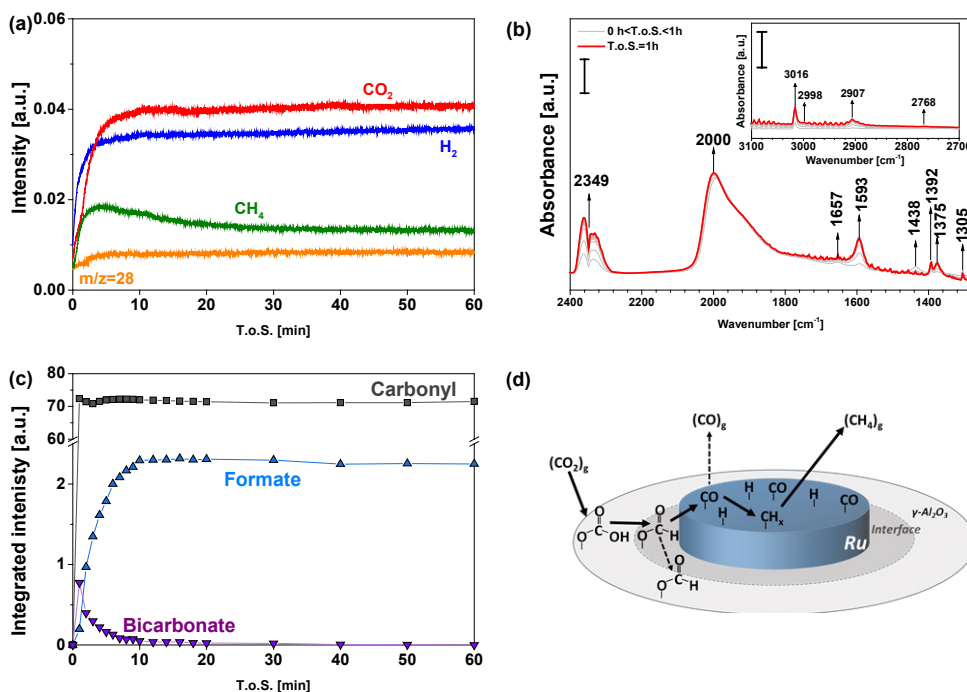
19 To better investigate the deactivation phenomena, a second set of CO/CO₂ co-feeding experiment was
 20 carried out by varying the temperature in the range of 290-400 °C at different CO/CO₂ inlet ratios. The
 21 results, displayed in **Figure S3** in the supplemental material, showed that the effect of CO addition is more
 22 evident at low temperature: the 2h-average deactivation rate observed during the CO/CO₂ co-feeding,
 23 showed in **Figure 2(b)**, increases with decreasing temperature.

1 3.3 *In situ* DRIFTS-MS measurements

2 In order to identify the key surface species during the methanation of CO₂, CO and CO/CO₂ mixtures, *in*
 3 *situ* DRIFTS-MS measurements were carried out at 200 °C using the homogeneously impregnated in-house
 4 prepared catalyst (*Ru-N*). The temperature was reduced with respect to the experiments reported in Section
 5 3.2, with the purpose of favoring the deactivation phenomena during the CO feed.

6 3.3.1. CO₂ hydrogenation

7 **Figure 3(a)** shows MS signals for the species leaving the DRIFT cell in the gas phase during CO₂
 8 hydrogenation. At T.o.S.=0 h CO₂ and H₂ were admitted to the reactor; the methane concentration shows a
 9 maximum at 5 min on stream, and then reaches a steady state value after 20 min. Evolution of the m/z=28
 10 signal is also observed, but this mostly results from the contribution of CO₂ fragmentation in the mass
 11 spectrometer.



12 **Figure 3** - CO₂ methanation at 200 °C: (a) MS signals for the gas phase as function of the T.o.S, (b) DRIFT spectra (inset 3100-2700 cm⁻¹
 13 wavenumber region), (c) corresponding intensity trends for the adsorbed species and (d) schematic representation of reaction pathway (solid
 14 arrows show the main paths). [Process conditions: T=200 °C, P=1 ata, F=15 mL/min, H₂/CO₂/He=8/2/90 molar ratios, catalyst: *Ru-N*]
 15

16 The corresponding recorded DRIFT spectra are shown in **Figure 3(b)**. The observed IR bands are related
 17 to species in gas phase, as well as adsorbed on both the Al₂O₃ support and the Ru particles. Specifically, IR
 18 features of gas phase CO₂ are centered at 2349 cm⁻¹, while the produced gas phase CH₄ shows the typical
 19 δ_{CH} bending vibrational feature at 1305 cm⁻¹ and the asymmetric ν_{C-H} stretching vibration at 3016 cm⁻¹ (see

1 inset). The rotational vibrational spectrum of gaseous water, the main byproduct of the Sabatier reaction, is
2 observed in the 1800–1300 cm^{-1} range.

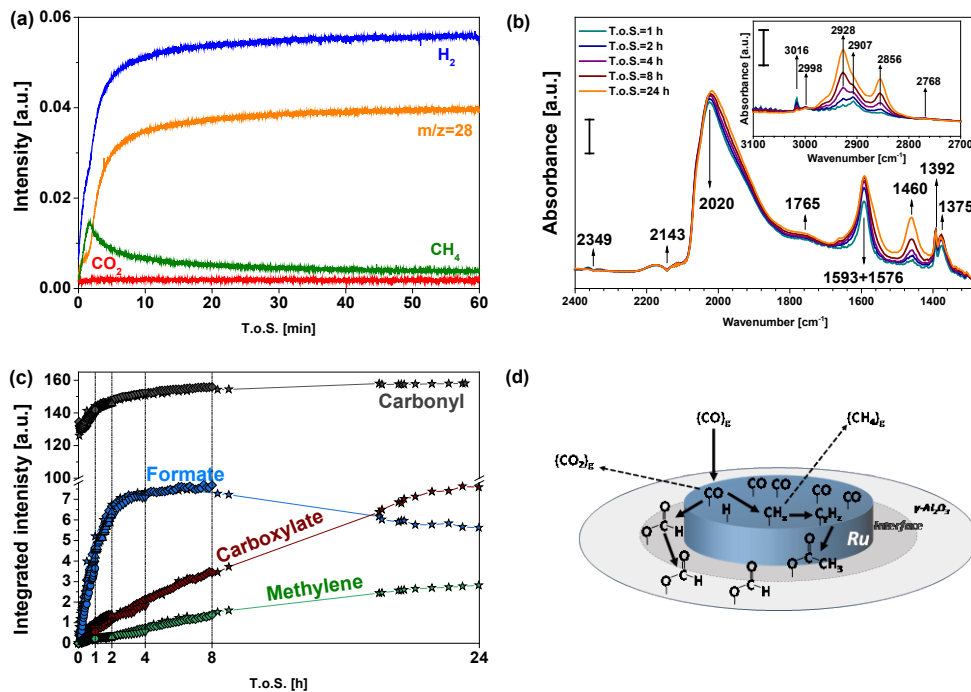
3 Focusing on the species adsorbed on the catalyst surface, the IR bands at 1657 and 1438 cm^{-1} represent the
4 asymmetric and symmetric OCO-stretching vibrations of the adsorbed bicarbonate species (in addition to
5 the OH deformation at 1228 cm^{-1} , not shown), formed upon reaction between CO_2 and the hydroxyl groups
6 of the Al_2O_3 support [34,62–65]. Furthermore, formate species are also detected, with bands at 1593, 1392
7 and 1375 cm^{-1} associated with the asymmetric OCO-stretching, CH-deformation and symmetric OCO-
8 stretching, respectively [43,55,66]. Additionally, the formates show a high wavenumber vibration at 2907
9 cm^{-1} , associated with the CH-stretching, and two peaks at 2998 and 2768 cm^{-1} , related to the combination
10 of vibrations previously described [66]. The complex peak in the range 2080–1800 cm^{-1} , with the maximum
11 at $\sim 2000 \text{ cm}^{-1}$, is assigned to carbonyls on the Ru-surface in multiple bonding configurations [30,44,55,67–
12 69]. Indeed, the shape and the lower wavenumber tail of this peak indicate that CO is not present only in
13 the linear configuration on the metallic Ru, but also in the bridging and three-folded configuration on
14 different coordination Ru sites.

15 The evolution of the detected species on the catalyst surface as function of T.o.S. is reported in terms of
16 integrated band intensities in **Figure 3(c)** (bicarbonate=1438 cm^{-1} , formate=1392+1375 cm^{-1} ,
17 carbonyl=2080–1800 cm^{-1}). The bicarbonate concentration shows a maximum and then decreases to a very
18 small steady state value. At variance, the concentration of formate species monotonically increases with
19 time on stream and reaches a steady state value. The broad band representing adsorbed CO reaches its
20 maximum almost instantaneously and retains its value during the entire analysis time. These trends are in
21 line with prior literature [54,55], sketched in **Figure 3(d)**: CO_2 is adsorbed on the catalyst support forming
22 bicarbonate species, which are hydrogenated to formates at the metal-support interface by hydrogen
23 dissociatively adsorbed on the metal sites. The formates can be further hydrogenated producing CO
24 adsorbed on the Ru sites or migrate and accumulates on the alumina support. The adsorbed CO is then
25 stepwise hydrogenated to methane rather than released in the gas phase, as suggested by the low CO
26 selectivity.

27 3.3.2. CO hydrogenation

28 The results obtained during the CO hydrogenation over the *Ru-N* catalyst sample are shown in **Figure 4**. In
29 this case the dynamics is slower than that of CO_2 and therefore, to better understand the phenomena
30 occurring on the catalyst surface, the length of the experiments was increased to 24 h.

31 **Figure 4(a)** shows the MS signals of the species outgoing the DRIFTS cell during the first hour on stream,
32 which describes the observed initial transient. The gas phase CH_4 signal shows a maximum after a few
33 minutes and then progressively decreases with decreasing slope with time on stream.



1
2 **Figure 4** - CO methanation at 200 °C: (a) MS signals for the gas phase as function of the T.o.S, (b) DRIFT spectra (inset 3100-2700 cm⁻¹
3 wavenumber region), (c) corresponding intensity trends for the adsorbed species and (d) schematic representation of reaction pathway (solid
4 arrows show the main paths). [Process conditions: T=200 °C, P=1 ata, F=15 mL/min, H₂/CO/He=8/2/90 molar ratios, catalyst: Ru-N]

5 The DRIFT spectra recorded during CO hydrogenation (**Figure 4(b)**) show significant differences with
6 respect to those recorded during CO₂ hydrogenation (**Figure 3(b)**). The gas phase CO bands, centered at
7 2143 cm⁻¹, are visible along with only very little amounts of gas phase CO₂ produced by the reaction, as
8 further confirmed by MS signals. Looking at the adsorbed surface species, bicarbonates are not observed
9 during the CO hydrogenation, while formates are much more abundant on the catalyst surface than on the
10 CO₂/H₂ gas stream (**Figure 3(b)**). Also, a new peak located at 1460 cm⁻¹ appears, which has been attributed
11 to the symmetric OCO-stretching of carboxylate groups (e.g. acetates) [36,70,71]. The asymmetric OCO-
12 stretching vibration of this species is located at ~1576 cm⁻¹, but it is masked by the feature of the formate
13 species at 1593 cm⁻¹. Literature reports the formation of carboxylates on alumina support by interaction of
14 hydrocarbons with the alumina hydroxyl groups [71,72]. Furthermore, in analogy to what reported in the
15 Fischer-Tropsch literature, although working at different process conditions, carboxylate species could also
16 be formed on the metal by insertion of CO during the hydrocarbon chain growth [73]. Nevertheless, on the
17 basis the adsorption of acetic acid on Ru(0001) [74], it is likely that the carboxylates are adsorbed, at least
18 partially, on the alumina.

19 The intensity of the carbonyl related bands in the range 2080÷1800 cm⁻¹ is strongly enhanced with respect
20 the case of CO₂ hydrogenation, suggesting that the CO coverage on ruthenium is enhanced by the presence
21 of CO in the feed stream. The appearance of the broad and weak band around 1765 cm⁻¹ suggests the

1 formation of bridged carbonyls, even though we cannot exclude that this band is due to another type of
2 surface species [75].

3 Two bands, not visible during CO₂ hydrogenation, are also detected in the CH-stretching region during CO
4 hydrogenation, in addition to those associated with formates and gas phase CH₄. They are centered at 2928
5 and 2856 cm⁻¹ and are both related to the stretching vibrations of methylene groups, indicating the presence
6 of methylene fragments (Ru=CH₂) and/or aliphatic hydrocarbons on the catalyst surface [36,70], most
7 probably on the Ru particles [44,76], even if some authors proposed the same features for hydrocarbons
8 adsorbed on the alumina surface [43]. Furthermore, because of the interference with the vibrational peaks
9 of the gas phase methane, for short time on stream it is not possible to observe another band at 2966 cm⁻¹
10 related to the methyl group [44,76], but it is clearly observable at T.o.S.=24 h.

11 The integrated intensities of the IR bands observed during CO hydrogenation are shown in **Figure 4(c)** as
12 a function of time on stream. The intensity of the multi-bonded carbonyl peak rapidly increases with T.o.S.,
13 especially during the first 2 h on stream. This seems to be related with the deactivation rate in CH₄ formation
14 as observed in the MS signal (**Figure 4(a)**). This behavior indicates that the coverage of the active sites by
15 CO increases during CO hydrogenation, progressively decreasing the number of active sites available for
16 the dissociative H₂ adsorption. It is speculated that this is one of the causes of the deactivation phenomena
17 observed during the CO hydrogenation, and is also in line with the observed kinetics of the CO methanation
18 showing positive order with respect the H₂ and negative order with respect the CO [35,41]. This also well
19 explains the reactivity behavior of the *Ru-SA* catalyst (**Figure 2**) which undergoes deactivation at low
20 temperature and high CO/CO₂ ratio in the gas feed, conditions that decrease the H/CO ratio on the catalyst
21 surface.

22 Besides carbonyls, the formate surface concentration increases during the first 2 h on stream, reaching a
23 maximum around 6-8 h, with an amount about three times higher than that observed during CO₂
24 hydrogenation. Then the concentration of formates slightly decreases with time on stream. Dalla Betta and
25 Shelef [43], based on their isotopic exchange experiments, reported that the formate species are not reaction
26 intermediates, but byproducts adsorbed on the alumina support (spectator species). It is worth to note that
27 the function of the formate species during CO hydrogenation is completely different from that in CO₂
28 methanation, where they are precursors of CO formation. Furthermore, Dalla Betta and Shelef [43] reported
29 that formates can be formed directly on the alumina surface from the reaction of H₂ and CO even in the
30 absence of metallic Ru. Besides, as suggested by Lorito et al. [70] for a similar catalyst, an additional route
31 for formate production is the spillover of CO from the metallic Ru sites to the alumina support. Based on
32 the observed evolution of the formate concentration, it is speculated that the concentration of these species
33 reaches a maximum due to saturation coverage of the alumina support, and then slightly decreases being

1 involved in the formation of other species bonded to the alumina surface (e.g., CH_x-containing surface
2 species).

3 **Figure 4(c)** also shows that the surface coverage of methylene species (calculated by integrating the 2856
4 cm⁻¹ band) linearly increases with the time on stream. Since no decrease in the CO coverage was observed
5 during the accumulation of these species, they are likely located only on a small portion of the metal surface.
6 During the experiments no hydrocarbons other than CH₄ were detected by MS in the gas phase. This
7 indicates that their concentration is too low to be detected and/or that, if produced, they remain adsorbed
8 on the catalyst surface. Eventually, the carboxylate species (whose trend was calculated by integrating the
9 1460 cm⁻¹ band) show a continuous concentration increase, reaching a near saturation value after 24 h on
10 stream.

11 Based on these evidences, it is suggested that CO is initially strongly adsorbed on Ru sites, progressively
12 reducing the active sites for the hydrogen dissociative adsorption (**Figure 4(d)**). The adsorbed CO can be
13 hydrogenated on metallic Ru to CH_x species (leading to methane) and other hydrocarbons, which remain
14 adsorbed on Ru. The reaction of CO with surface hydroxyls may also lead to formate species at the
15 Ru/Al₂O₃ interface that can spill over the alumina support. Carboxylate species can also be formed, upon
16 reaction of hydrocarbons with alumina hydroxyls groups. These species likely remain adsorbed at the
17 Ru/Al₂O₃ interface. Finally, small amounts of gas phase CO₂ are also produced, due to the occurrence of
18 the water gas shift reaction.

19 3.3.3. CO/CO₂ hydrogenation

20 Finally, DRIFTS-MS experiments were performed during the CO/CO₂ methanation. As shown in **Figure**
21 **5(a)**, in these experiments the reactivity of CO₂/H₂ was initially investigated (T.o.S.=0-20 min) and then,
22 after a He purge, the feed was switched to CO/CO₂/H₂ (T.o.S.=30-70 min). Eventually, the reactivity of
23 CO₂/H₂ was investigated again (T.o.S.=80-100 min).

24 The DRIFT spectra of the surface, recorded at relevant T.o.S. (20, 70 and 100 min), i.e. at the end of each
25 different feed, are shown in **Figure 5(b)**, while **Figure S4** provides the complete series of IR spectra
26 collected during the whole experiment.

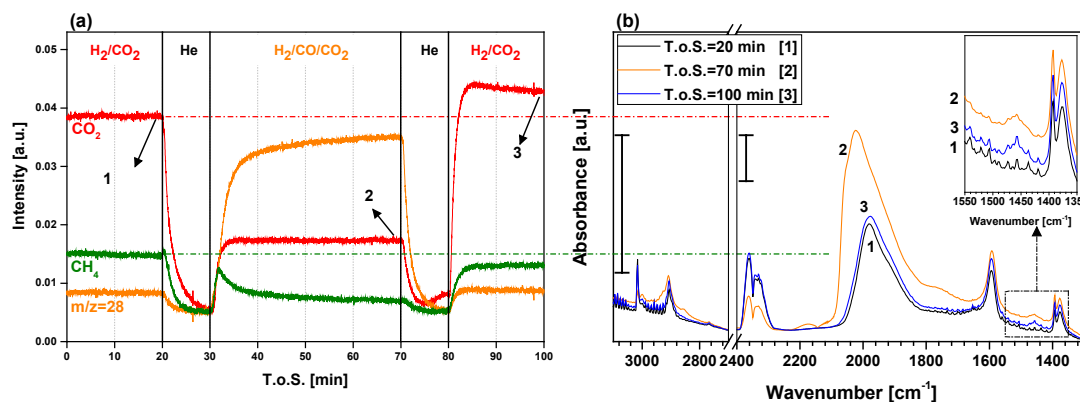


Figure 5 - (a) MS signals and (b) DRIFT spectra collected during the CO_x methanation at T=200 °C.

[Process conditions: P=1 ata, F=15 mL/min, H₂/CO₂/He=8/2/90 (cond. 1, 3), H₂/CO/CO₂/He=8/1.6/0.4/90 (cond. 2), catalyst: Ru-N]

Spectrum 1 of **Figure 5(b)** shows the species during CO₂ hydrogenation, and accordingly multi-bonded CO and formates are adsorbed on the catalyst surface, as previously discussed. By introducing CO into the gas feed (T.o.S.=30-80 min) the catalyst is deactivated, as shown by the MS signal of CH₄ in **Figure 5(a)**. At the end of this period (spectrum 2 in **Figure 5(b)**, T.o.S.=70 min), the concentration of the adsorbed CO is greatly increased, reaching an intensity similar to the case of pure CO hydrogenation (**Figure 4(b)**). Furthermore, during this period, the formate intensity is also increased and IR bands characteristic of hydrocarbons and carboxylates appear (inset of **Figure 5(b)**). As a matter of facts, the behavior of the catalyst during CO/CO₂ hydrogenation is similar to that observed during hydrogenation of pure CO and described in **Figure 4**.

By returning to CO₂ hydrogenation process conditions (T.o.S.=80-100 min), the catalyst shows a loss of activity as pointed out by the MS signals of CH₄ and CO₂. The corresponding IR spectrum (spectrum 3 in **Figure 5(b)**) shows that the CO band decreases back to the intensity of spectrum 1, and the bands of methylene groups cannot be observed. In contrast, the formate and carboxylate peaks retain their intensities during the whole period. Accordingly, the main difference between the surface observed during CO₂ hydrogenation on fresh catalyst and the deactivated one (i.e. after CO/CO₂ hydrogenation) is the presence, in the latter case, of the bands of carboxylate species (**inset-Figure 5(b)**).

The same set of experiments has been repeated at a higher temperature, 250 °C, and results are shown in **Figure 6(a)** (MS signal intensities) and **Figure 6(b)** (representative IR spectra, while the complete series of experimental data is reported in **Figure S5**).

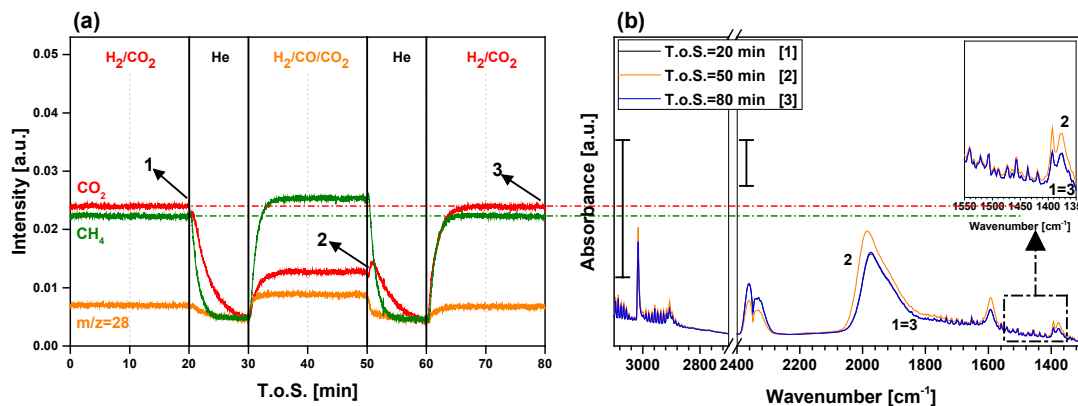


Figure 6 - (a) MS signals and (b) DRIFT spectra collected during the CO_x methanation at T=250 °C.

[Process conditions: P=1 ata, F=15 mL/min, H₂/CO₂/He=8/2/90 (cond. 1, 3), H₂/CO/CO₂/He=8/1.6/0.4/90 (cond. 2), catalyst: Ru-N]

1
2
3
4 As expected, the CH₄ productivity increases upon increasing the temperature during CO₂ hydrogenation
5 (T.o.S.=0-20 min), as can be seen from the comparison of the MS signal of CH₄ in **Figure 6(a)** and **Figure**
6 **5(a)**. Focusing on the species adsorbed on the catalyst surface (spectrum 1 in **Figure 6(b)**), the amounts of
7 carbonyls and formates decrease at this temperature with respect the experiment carried out at lower
8 temperature. Switching to H₂/CO/CO₂ gas feed (T.o.S.=30-50 min), the catalyst shows stable performance
9 and, moreover, the amount of methane produced increases with respect to the pure CO₂ hydrogenation. The
10 IR spectrum collected at the end of CO/CO₂ co-feeding period (spectrum 2 in **Figure 6(b)**) shows that the
11 bands related to CO are only slightly increased in the presence of CO. This behavior is due to the twofold
12 effect of temperature, i.e. reduces the CO adsorption and increases the rate of adsorbed CO hydrogenation.
13 Furthermore, no CH_x and carboxylate species are observed on the catalyst surface at 250 °C. After switching
14 back to pure CO₂ hydrogenation (T.o.S.=60-80 min) both the gas phase composition and the surface species
15 are the same observed for the fresh catalyst (compare spectrum 1 and 3 in **Figure 6(b)**).
16 These results are in agreement with the reactivity data collected in the fixed bed reactor for the *Ru-SA*
17 catalyst (**Figure S3(b)**), although the process conditions were somewhat different. In fact, also in this case
18 operating at high temperature reduces deactivation of Ru-based catalysts during CO/CO₂ methanation.
19 **Figure 7** sketches the state of the catalyst surface during the CO/CO₂ methanation. By working at low
20 temperature, CO is strongly adsorbed on the Ru sites and methylene groups and carboxylate species are
21 produced on the catalyst surface, progressively reducing the hydrogenating capability of the catalyst and
22 blocking the CO₂ methanation. Working at high temperature reduces the amounts of adsorbed CO on Ru
23 and is quantitatively converted to methane. No carboxylates and hydrocarbons are observed, whose
24 presence is blamed for catalyst deactivation. Very likely, the high hydrogenation activity at high
25 temperature keeps clean the catalyst surface, allowing the CO_x methanation pathways to occur.

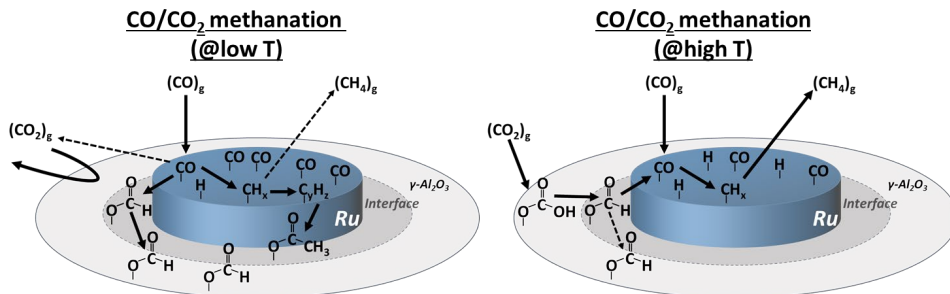


Figure 7 – Schematic representation of the catalyst surface during CO/CO₂ methanation (solid arrows show main paths)

3.4. Reactivity of the adsorbed surface species

To better clarify the picture, the reactivity of the adsorbed species formed during the CO_x hydrogenation at 200 °C was investigated in the presence of H₂ at the same temperature. The catalyst surface after pure CO hydrogenation was chosen as starting point because all the important adsorbed species were present. IR spectra collected during this hydrogenation are reported in **Figure 8(a)**, while in **Figure 8(b)** the decay of integrated intensities of the bands of adsorbed species is plotted in a log scale.

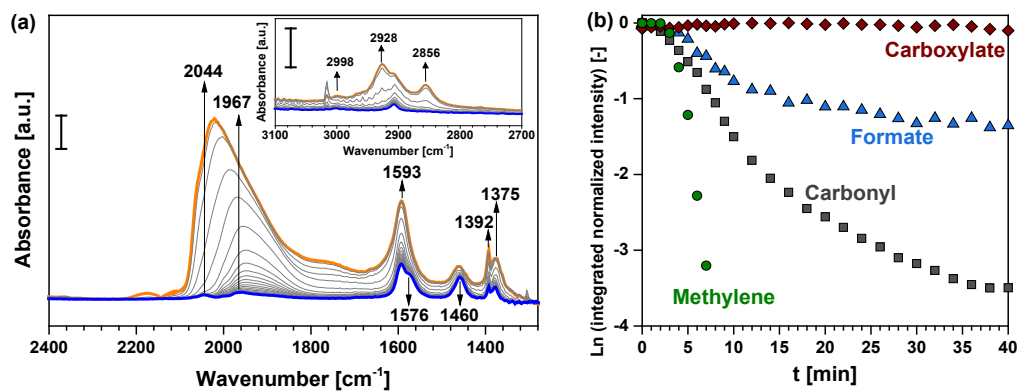


Figure 8 - (a) DRIFT spectra collected during a 40 min long hydrogenation treatment carried out after 8 h on stream of H₂/CO at T=200 °C.

(b) The natural logarithm decay for the adsorbed species during the hydrogenation step.

[Process conditions: T=200 °C, P=1 ata, F=15 mL/min, H₂/CO/He=8/2/90 or H₂/ He=8/92 molar ratios, catalyst: Ru-N]

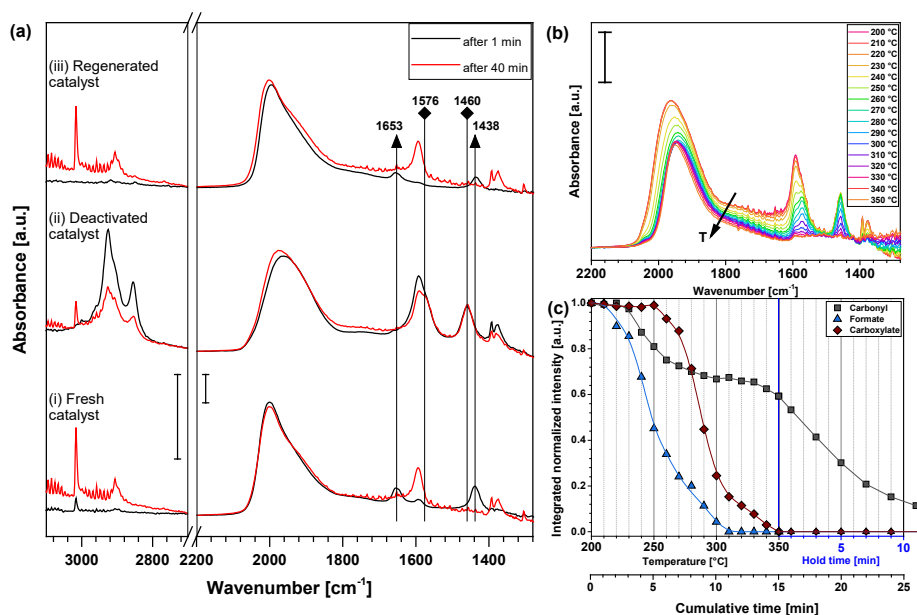
As apparent from **Figure 8**, the most reactive species are the methylene groups, as the intensity of their characteristic band intensity quickly decays and disappear after about 5 min under H₂. The high reactivity of these species confirms their location on the Ru sites rather than on the Al₂O₃ support [44,76]. Furthermore, considering that these species are highly reactive with H₂, the increase of their concentration that is observed during the CO and CO/CO₂ methanation indicates the shortage of active hydrogen on the ruthenium surface under the process conditions applied in this study. In fact, the only product detected by the MS is methane, meaning that adsorbed CH_x fragments are easily hydrogenated to methane. Also the carbonyl band intensity almost completely disappears during the hydrogenation treatment, although with a slower rate. Looking at the temporal evolution of the IR features of adsorbed CO (**Figure 8(a)**), a shift of the maximum from 2022 cm⁻¹ to 1951 cm⁻¹ can be observed, due to the decrease in the CO

1 coverage. New features become also visible in the adsorbed CO band, and in particular two peaks become
2 detectable at 2044 and 1967 cm^{-1} , related to geminal di-carbonyls adsorbed on low coordination Ru sites,
3 where the hydrogenation is less favored [55]. The presence of these stable carbonyl species justifies the
4 trend for the overall CO species intensity observed in **Figure 8(b)**, which does not follow a complete
5 straight logarithmic decay, indicating that reactivity of carbonyl species is not uniform. The presence of
6 these less reactive and highly stable species may be considered an additional cause of deactivation.
7 Eventually, a CO supply contribution, coming from the formate hydrogenation and delaying carbonyl
8 decay, has to be considered.

9 The decay curve of the formate species shows two distinct slopes: up to 10 min the slope is steep (high
10 kinetic rate constant), followed by a slower process after about 10 min. As already reported in the literature
11 for both CO_2 [54,55] and CO [77] methanation, this suggests that two types of formates are present. They
12 are commonly classified as “fast” and “slow” formates, depending on their distance from the Ru particles.
13 Formates close to the Ru particles (source of active hydrogen) react faster than those far away from the
14 metal particles. It is worth noticing that the trends of formate and carbonyl intensities are similar, in that
15 both show a change in the decay slope. This behavior supports the correlation existing between these
16 species, where formates are intermediates of carbonyl formation when CO is not fed into the reactor (i.e.
17 during CO_2 methanation).

18 Finally, the trend of the carboxylate species differs from that of all other species, since it does not show any
19 decay during the H_2 treatment at 200 °C. As a result, the peak at 1576 cm^{-1} , associated with the asymmetric
20 OCO-stretching of carboxylates, becomes visible due to the gradual disappearance of the 1593 cm^{-1} peak
21 associated with the formates. Notably, the very different behaviors of the OCO-carboxylate vibrations and
22 the methylene peaks indicates that these two fragments are unlikely related.

23 The reactivity of adsorbed species was additionally analyzed by carrying out experiments with a $\text{H}_2/\text{CO}_2=1$
24 feed stream, in order to slow down the evolution of the adsorbed species. In fact, in this way the bicarbonate
25 species can be used as probe to check surface coverages on the alumina support, being this species certainly
26 located on alumina [34,62–65]. Accordingly, experiments were carried out at 200 °C (i) on the fresh catalyst
27 and (ii) on the catalyst that was previously deactivated in H_2/CO gas mixture for 24 h. IR spectra collected
28 in these cases after 1 min and 40 min (black and red spectra, respectively) during the H_2/CO_2 reaction are
29 presented in **Figure 9(a)**. The figure also shows the spectra obtained in the case of a “regenerated” sample,
30 which will be discussed later on.



1
2 **Figure 9** - (a) DRIFT spectra in the CO₂ hydrogenation on the catalyst previously treated: (i) fresh, (ii) deactivated by flowing H₂/CO/He=8/2/90
3 for 24 h at 200 °C; (iii) regenerated by flowing pure He at 350 °C, heating ramp 10°C/min and hold for 20 min.
4 (b) DRIFT spectra and (c) adsorbed species intensity decay during the regeneration treatment.
5 [Process conditions: T=200 °C, P=1 ata, F=15 mL/min, H₂/CO₂/He=5/5/90, catalyst: Ru-N]

6
7 In the case of the fresh sample (case i), after 1 min on stream in H₂/CO₂=1 (black spectrum in **Figure 9(a)**),
8 the IR features of bicarbonates adsorbed on the alumina surface are significantly higher than those observed
9 in the case of the H₂/CO₂=4 flow (**Figure 3(b)**). However, after 40 min on stream (red spectrum), the surface
10 species formed are similar to those observed with the H₂/CO₂=4 gas feed.

11 After the extensively deactivating treatment (case ii), methane formation during CO₂ hydrogenation is much
12 lower, as confirmed by the intensity of the ν_{C-H} vibration of gas phase CH₄ at 3610 cm⁻¹ (**Figure 9(a)**). IR
13 features of hydrocarbon, formate, carboxylate and carbonyl species are clearly seen, however no
14 bicarbonates are detectable, not after 1 minute on stream (black spectrum). This indicates that a portion of
15 the alumina surface is blocked. After 40 min in the H₂/CO₂ gas mixture (red spectrum), the presence of
16 hydrocarbons on the catalyst is still evident, although their intensities are effectively reduced, indicating a
17 hydrogenation of these species during CO₂ methanation. Most importantly, no change occurs in the IR
18 intensity of carboxylate feature, while that of the formates decreases with T.o.S. indicating their
19 participation in the methanation reaction. All these results suggest that carboxylates block alumina sites
20 participating in the CO₂ reduction by preventing the formation of bicarbonates. Besides, inspection of the
21 IR spectra reveals that the shape of the carbonyl peak is slightly different during CO₂ hydrogenation over
22 the fresh and the deactivated sample, as a shoulder is present near 1975 cm⁻¹ in the case of the deactivated
23 sample (case ii). This is likely associated to the influence of other surface species (i.e., carboxylates and/or

1 hydrocarbons) in the proximity of Ru sites, which modifies the adsorption strength of CO on the ruthenium
2 particles.

3 With the aim of recovering the catalyst reactivity, a regeneration treatment (heating under inert gas from
4 200°C to 350°C) was carried out. The IR spectra collected during this treatment are shown in **Figure 9(b)**
5 as a function of temperature, along with the intensity of the normalized integrated IR bands (**Figure 9(c)**).
6 The decomposition of formates (triangles) starts at 220 °C and their characteristic IR bands completely
7 disappear at 310 °C. The onset temperature for the carboxylate decomposition is observed at higher
8 temperatures, above 250°C, indicating their higher thermal stability. The decay of the bands of adsorbed
9 CO is somewhat peculiar, showing a two-step decrease with a steady level in the 250-350°C temperature
10 range. A comparison of this trend with that of the carboxylate species suggests that the decomposition of
11 carboxylates, characterized by a higher onset temperature, supplies CO to the Ru particles, and this leads
12 to a decrease in the rate of the decrease of the carbonyl band. This may also indicate that carboxylate species
13 are located near to the ruthenium sites, probably at the metal/support interface, differently from “slow
14 formate” that are located far from the metal sites. This is in line with the reported carboxylate formation
15 pathway assuming that hydrocarbons formed on the metal particles spill over to adsorption sites on alumina
16 [71,72]. Carboxylates located in this position may also affect the peak shape of the adsorbed carbonyls as
17 observed during CO₂ hydrogenation on the deactivated catalyst.

18 Eventually, the IR spectra were collected during CO₂ methanation over the regenerated catalyst (i.e. after
19 heating under He flow) and results are shown in **Figure 9(a)** (case iii). These spectra are very similar to
20 those recorded in the case of the fresh sample; in particular the spectrum collected after 1 min in the H₂/CO₂
21 feed (black curve) clearly shows the presence of bicarbonates, indicating that the alumina surface is
22 recovered during the high temperature regeneration in He, by decomposing and desorbing the carboxylate
23 species.

24 The ability to totally recover the catalyst reactivity by increasing the temperature under inert gas flow was
25 also confirmed by reactivity studies on both *Ru-SA* and *Ru-N* catalysts, as reported by **Figure S6**. These
26 results point out that the temperature is the crucial parameter for catalyst regeneration, suggesting that
27 activity recovery is mainly due to decomposition/conversion and/or desorption of C-containing species
28 accumulated on the catalyst surface during CO methanation at low temperature. Furthermore, considering
29 that catalytic activity can be completely recovered upon flowing an inert gas at high temperature, the
30 deposition of carbon and/or formation of carbide on the catalyst surface (species not detectable with IR
31 spectroscopy) seems to be unlikely the main reason of deactivation under the analyzed process conditions.
32 Eventually the spent *Ru-N* catalyst, deactivated by carrying CO methanation for 24 h, was analyzed by *ex*
33 *situ* TEM imaging, after an *in situ* passivation step at room temperature by flowing 2 vol.% O₂ in N₂. The
34 results, reported in **Figure S2**, show that the average size of Ru particles is only slightly increased after

1 CO_x hydrogenation, although it is characterized by a more broadened size distribution than the fresh
2 catalyst. However, since the catalyst activity is totally reversible, Ru sintering is excluded as main cause of
3 deactivation. In contrast, the formation of very stable carboxylate species, produced only in the presence of
4 CO in the gas feed seems to have a key role in the deactivation of the catalyst during CO₂ hydrogenation.

5 **4. Conclusion**

6 In this work the reactivity of commercial and home-made Ru/Al₂O₃ catalysts in the CO/CO₂ methanation
7 was investigated. Mechanistic aspects of the reaction were also investigated by DRIFTS experiments, and
8 particular attention was paid on the reaction pathways and on the deactivation phenomena occurring when
9 CO is present in the reacting mixture along with CO₂.

10 Both the catalysts are stable and highly selective in the CO₂ methanation. The presence of CO in the reacting
11 CO₂/H₂ mixture at low temperatures leads to a decrease in the CO₂ conversion and, at high CO
12 concentrations, a progressive deactivation of the catalyst. When switching the feed back to the CO-free
13 atmosphere, a permanent deactivation is observed for high CO concentrations.

14 DRIFTS experiments, carried out over the home-made catalyst, show that the CO₂ hydrogenation reaction
15 pathway is in line with that reported in the literature: carbon dioxide is adsorbed on the support as
16 bicarbonate and is progressively hydrogenated to methane passing through the formation of formate
17 adsorbed at the metal-support interface, and of carbonyl species on the metallic ruthenium surface.

18 When CO is present in the gas feed, the reaction sites for CO₂ hydrogenation are blocked by CO and the
19 catalysts show deactivation, when operated at low temperature. The extent of activity loss increases upon
20 increasing the CO/CO₂ ratio in the inlet gas stream and upon decreasing the catalyst temperature, thus
21 suggesting a CO self-inhibition mechanism.

22 DRIFTS experiments confirm that, in the presence of gas phase CO in the feed, the CO coverage is higher
23 on the catalyst surface than that during methanation in pure CO₂. As the CO coverage becomes high on the
24 Ru particles, the methanation becomes kinetically inhibited due to the decrease of hydrogen concentration
25 on the metal sites. Additionally, carbonyls with different hydrogenation kinetics are detected on the Ru
26 sites, showing the presence of species having poor reactivity, e.g. geminal di-carbonyls on well-dispersed
27 sites. Notably, in the presence of CO in the gas feed, formates, carboxylates and hydrocarbons are formed
28 and deposited on the catalyst surface. They exhibit different reactivity, with carboxylates showing the
29 highest stability. Indeed, while hydrocarbons and formates can be removed by hydrogenation, carboxylates
30 are very stable and cannot be removed. These stable oxide-bound surface species block adsorption sites for
31 CO₂, thus lowering the CO₂ methanation activity of the catalyst even after the removal of CO from the gas
32 feed stream. The observed deactivation, however, is reversible. By increasing the process temperature, even

1 in inert gas flow, the catalyst activity can be completely recovered, due primarily to the thermal
2 decomposition of the carboxylate species.

3 In conclusion, methanation in CO/CO₂ co-feed can be effectively carried out on Ru-based catalysts by
4 working at temperatures high enough to prevent high CO coverage and the formation of stable carboxylate
5 species, whose presence is the reason for catalyst deactivation.

6 **Acknowledgments**

7 Catalyst preparation, characterization and testing activity were carried out with a joint project between the
8 Politecnico di Milano and the Italian National Agency for New Technologies, Energy and Sustainable
9 Economic Development (ENEA), which is gratefully acknowledged. The authors gratefully acknowledge
10 the financial support of the DRIFTS experiments by the US Department of Energy (DOE), Office of
11 Science, Office of Basic Energy Sciences, Chemical Sciences, Geosciences, and Biosciences Division. L.F.
12 also acknowledges the Pacific Northwest National Laboratory (PNNL) for the financial support during his
13 stay as a visiting student.

14 **Supporting Information**

15 Additional figures: TEM images, activity data, DRIFT and mass spectra.

16 **References**

- 17 [1] K.M.K. Yu, I. Curcic, J. Gabriel, S.C.E. Tsang, Recent advances in CO₂ capture and utilization., *ChemSusChem*. 1 (2008) 893–9.
18 doi:10.1002/cssc.200800169.
- 19 [2] M. Aresta, A. Dibenedetto, A. Angelini, Catalysis for the Valorization of Exhaust Carbon: from CO₂ to Chemicals, Materials, and Fuels.
20 Technological Use of CO₂, *Chem. Rev.* 114 (2014) 1709–42. doi:10.1021/cr4002758.
- 21 [3] B. Kumar, J.P. Brian, V. Atla, S. Kumari, K.A. Bertram, R.T. White, et al., New trends in the development of heterogeneous catalysts
22 for electrochemical CO₂ reduction, *Catal. Today*. 270 (2016) 19–30. doi:10.1016/j.cattod.2016.02.006.
- 23 [4] W. Wang, S. Wang, X. Ma, J. Gong, Recent advances in catalytic hydrogenation of carbon dioxide., *Chem. Soc. Rev.* 40 (2011) 3703–
24 27. doi:10.1039/c1cs15008a.
- 25 [5] K. Li, X. An, K. Hyeon, M. Khraisheh, J. Tang, A critical review of CO₂ photoconversion : Catalysts and reactors, *Catal. Today*. 224
26 (2014) 3–12. doi:10.1016/j.cattod.2013.12.006.
- 27 [6] IEA, Energy Technology Perspectives 2017 - Catalysing Energy Technology Transformations, 2016. www.iea.org/etp2017.
- 28 [7] IPCC, Climate Change 2014: Synthesis Report, Geneva, Switzerland, 2014. doi:10.1017/CBO9781107415324.
- 29 [8] V. Barbarossa, C. Bassano, P. Deiana, G. Vanga, CO₂ Conversion to CH₄, in: M. de Falco, G. Iaquaniello, G. Centi (Eds.), *CO₂ A Valuab.*
30 *Source Carbon*, Springer-Verlga, 2013: pp. 123–145. doi:10.1007/978-1-4471-5119-7.
- 31 [9] J. Gao, Q. Liu, F. Gu, B. Liu, Z. Zhong, F. Su, Recent advances in methanation catalysts for the production of synthetic natural gas, *RSC*
32 *Adv.* 5 (2015) 22759–22776. doi:10.1039/C4RA16114A.
- 33 [10] M.A.A. Aziz, A.A. Jalil, S. Triwahyono, A. Ahmad, CO₂ Methanation over Heterogeneous Catalysts: Recent Progress and Future
34 Prospects, *Green Chem.* 17 (2015) 2647–2663. doi:10.1039/C5GC00119F.
- 35 [11] M. Bailera, P. Lisbona, L.M. Romeo, S. Espatolero, Power to Gas projects review: Lab, pilot and demo plants for storing renewable
36 energy and CO₂, *Renew. Sustain. Energy Rev.* 69 (2017) 292–312. doi:10.1016/j.rser.2016.11.130.
- 37 [12] S. Rönsch, J. Schneider, S. Matthischke, M. Schlüter, M. Götz, J. Lefebvre, et al., Review on methanation - From fundamentals to current
38 projects, *Fuel*. 166 (2016) 276–296. doi:10.1016/j.fuel.2015.10.111.

- 1 [13] M. Götz, J. Lefebvre, F. Mörs, A. McDaniel Koch, F. Graf, S. Bajohr, et al., Renewable Power-to-Gas: A technological and economic
2 review, *Renew. Energy*. 85 (2016) 1371–1390. doi:10.1016/j.renene.2015.07.066.
- 3 [14] F.D. Meylan, V. Moreau, S. Erkman, Material constraints related to storage of future European renewable electricity surpluses with CO₂
4 methanation, *Energy Policy*. 94 (2016) 366–376. doi:10.1016/j.enpol.2016.04.012.
- 5 [15] T. Schaaf, J. Grünig, M.R. Schuster, T. Rothenfluh, A. Orth, Methanation of CO₂-storage of renewable energy in a gas distribution
6 system, *Energy. Sustain. Soc.* 4 (2014) 1–14. doi:10.1186/s13705-014-0029-1.
- 7 [16] P. Sabatier, J.B. Senderens, Nouvelle synthèse du méthane, *C. R. Acad. Sci. Paris*. 134 (1902) 514–516.
- 8 [17] J. Kopyscinski, T.J. Schildhauer, S.M.A. Biollaz, Production of synthetic natural gas (SNG) from coal and dry biomass - A technology
9 review from 1950 to 2009, *Fuel*. 89 (2010) 1763–1783. doi:10.1016/j.fuel.2010.01.027.
- 10 [18] T.A. Napp, A. Gambhir, T.P. Hills, N. Florin, P.S. Fennell, A review of the technologies , economics and policy instruments for
11 decarbonising energy-intensive manufacturing industries, *Renew. Sustain. Energy Rev.* 30 (2014) 616–640.
12 doi:10.1016/j.rser.2013.10.036.
- 13 [19] G.A. Mills, F.W. Steffgen, Catalytic Methanation, *Catal. Rev. Sci. Eng.* 8 (1974) 159–210. doi:10.1080/01614947408071860.
- 14 [20] I. Czekaj, F. Loviat, F. Raimondi, J. Wambach, S. Biollaz, A. Wokaun, Characterization of surface processes at the Ni-based catalyst
15 during the methanation of biomass-derived synthesis gas: X-ray photoelectron spectroscopy (XPS), *Appl. Catal. A Gen.* 329 (2007) 68–
16 78. doi:10.1016/j.apcata.2007.06.027.
- 17 [21] C. Mirodatos, H. Praliaud, M. Primet, Deactivation of nickel-based catalysts during CO methanation and disproportionation, *J. Catal.* 107
18 (1987) 275–287. doi:10.1016/0021-9517(87)90294-6.
- 19 [22] M. Agnelli, M. Kolb, C. Nicot, C. Mirodatos, Sintering of a Ni-based catalyst during CO hydrogenation: kinetics and modeling, in: C.H.
20 Bartholomew, J.B. Butt (Eds.), *Catal. Deactiv.*, Elsevier B.V, Amsterdam, 1991: pp. 605–612.
- 21 [23] B. Miao, S.S.K. Ma, X. Wang, H. Su, S.H. Chan, Catalysis mechanisms of CO₂ and CO methanation, *Catal. Sci. Technol.* 6 (2016) 4048–
22 4058. doi:10.1039/C6CY00478D.
- 23 [24] J.G. McCarty, H. Wise, Hydrogenation of Surface Carbon on Alumina-Supported Nickel, *J. Catal.* 57 (1979) 406–416. doi:10.1016/0021-
24 9517(79)90007-1.
- 25 [25] S. Helveg, C. López-Cartes, J. Sehested, P.L. Hansen, B.S. Clausen, J.R. Rostrup-Nielsen, et al., Atomic-scale imaging of carbon
26 nanofibre growth, *Nature*. 427 (2004) 5–8. doi:10.1038/nature02308.1.
- 27 [26] R.B. Anderson, *The Fischer Tropsch Synthesis*, Academic Press, Orlando, 1984.
- 28 [27] C. Janke, M.S. Duyar, M. Hoskins, R.J. Farrauto, Catalytic and adsorption studies for the hydrogenation of CO₂ to methane, *Appl. Catal.*
29 *B Environ.* 152–153 (2014) 184–191. doi:10.1016/j.apcatb.2014.01.016.
- 30 [28] J.H. Kwak, L. Kovarik, J. Szanyi, CO₂ Reduction on Supported Ru/Al₂O₃ Catalysts: Cluster Size Dependence of Product Selectivity,
31 *ACS Catal.* 3 (2013) 2449–2455. doi:10.1021/cs400381f.
- 32 [29] M. Marwood, R. Doepper, M. Prairie, A. Renken, Transient Drift Spectroscopy for the Determination of the Surface-Reaction Kinetics
33 of CO₂ Methanation, *Chem. Eng. Sci.* 49 (1994) 4801–4809. doi:10.1016/S0009-2509(05)80060-0.
- 34 [30] P. Panagiotopoulou, D.I. Kondarides, X.E. Verykios, Mechanistic Study of the Selective Methanation of CO over Ru/TiO₂ Catalyst:
35 Effect of Metal Crystallite Size on the Nature of Active Surface Species and Reaction Pathways, *J. Phys. Chem. C*. 121 (2017) 5058–
36 5068. doi:10.1021/acs.jpcc.6b12091.
- 37 [31] S. Sharma, Z. Hu, P. Zhang, E.W. McFarland, H. Metiu, CO₂ methanation on Ru-doped ceria, *J. Catal.* 278 (2011) 297–309.
38 doi:10.1016/j.jcat.2010.12.015.
- 39 [32] D.C. Upham, A.R. Derk, S. Sharma, H. Metiu, E.W. McFarland, CO₂ methanation by Ru-doped ceria: the role of the oxidation state of
40 the surface, *Catal. Sci. Technol.* 5 (2015) 1783–1791. doi:10.1039/C4CY01106F.
- 41 [33] L. Falbo, M. Martinelli, C.G. Visconti, L. Lietti, C. Bassano, P. Deiana, Kinetics of CO₂ methanation on a Ru-based catalyst at process
42 conditions relevant for Power-to-Gas applications, *Appl. Catal. B Environ.* 225 (2018) 354–363.
43 doi:doi.org/10.1016/j.apcatb.2017.11.066.
- 44 [34] G. Garbarino, D. Bellotti, E. Finocchio, L. Magistri, G. Busca, Methanation of carbon dioxide on Ru/Al₂O₃: Catalytic activity and infrared
45 study, *Catal. Today*. 277 (2016) 21–28. doi:10.1016/j.cattod.2015.12.010.
- 46 [35] F.S. Kam, J.F. Shultz, R.B. Anderson, Hydrogenation of Carbon Monoxide and Carbon Dioxide on Supported Ruthenium Catalysts at
47 Moderate Pressures, *Ind. Eng. Chem. Prod. Res. Dev.* 4 (1965) 265–269. doi:10.1021/i360016a014.

- 1 [36] J.M.G. Carballo, E. Finocchio, S. García-Rodríguez, M. Ojeda, J.L.G. Fierro, G. Busca, et al., Insights into the deactivation and
2 reactivation of Ru/TiO₂ during Fischer-Tropsch synthesis, *Catal. Today*. 214 (2013) 2–11. doi:10.1016/j.cattod.2012.09.018.
- 3 [37] C.H. Bartholomew, Mechanisms of catalyst deactivation, *Appl. Catal. A Gen.* 212 (2001) 17–60. doi:10.1016/S0926-860X(00)00843-7.
- 4 [38] H. Abrevaya, M.J. Cohn, W.M. Targos, H.J. Robota, Structure sensitive reactions over supported ruthenium catalysts during Fischer-
5 Tropsch synthesis, *Catal. Letters*. 7 (1990) 183–195. doi:10.1007/BF00764501.
- 6 [39] J.G. Goodwin, D.O. Goa, S. Erdal, F.H. Rogan, Reactive metal volatilization from Ru/Al₂O₃ as a result of ruthenium carbonyl formation,
7 *Appl. Catal.* 24 (1986) 199–209. doi:10.1016/S0166-9834(00)81268-3.
- 8 [40] Mukkavilli, Tavlarides, Wittmann, Tavlarides, Carbon Deactivation of Fischer-Tropsch Ruthenium Catalyst., *Ind. Eng. Chem. Process*
9 *Des. Dev.* 25 (1983) 45. doi:10.1021/i200033a023.
- 10 [41] R.A. Dalla Betta, A.G. Piken, M. Shelef, Heterogeneous Methanation: Steady-State Rate of CO Hydrogenation on Supported Ruthenium,
11 Nickel and Rhenium, *J. Catal.* 40 (1975) 173–183.
- 12 [42] R.M. Bowman, C.H. Bartholomew, Deactivation by Carbon of Ru/Al₂O₃ during CO hydrogenation, *Appl. Catal.* 7 (1983) 179–187.
- 13 [43] R.A. Dalla Betta, M. Shelef, Heterogeneous Methanation: In Situ Infrared Spectroscopic Study of Ru/Al₂O₃ during the Hydrogenation of
14 CO, *J. Catal.* 48 (1977) 111–119. doi:10.1016/0021-9517(77)90082-3.
- 15 [44] J.G. Ekerdt, A.T. Bell, Synthesis of hydrocarbons from CO and H₂ over silica-supported Ru: Reaction rate measurements and infrared
16 spectra of adsorbed species, *J. Catal.* 58 (1979) 170–187. doi:10.1016/0021-9517(79)90255-0.
- 17 [45] B.T. Loveless, C. Buda, M. Neurock, E. Iglesia, CO chemisorption and dissociation at high coverages during CO hydrogenation on Ru
18 catalysts, *J. Am. Chem. Soc.* 135 (2013) 6107–6121. doi:10.1021/ja311848e.
- 19 [46] D.L. King, An in Situ Infrared Study of CO hydrogenation over Silica and Alumina-Supported Ruthenium and Silica-Supported Iron, *J.*
20 *Catal.* 61 (1980) 77–86.
- 21 [47] N.W. Cant, A.T. Bell, Studies of carbon monoxide hydrogenation over ruthenium using transient response techniques, *J. Catal.* 73 (1982)
22 257–271. doi:10.1016/0021-9517(82)90099-9.
- 23 [48] P. Panagiotopoulou, D.I. Kondarides, X.E. Verykios, Mechanistic Study of the Selective Methanation of CO over Ru/TiO₂ Catalyst:
24 Identification of Active Surface Species and Reaction Pathways, *J. Phys. Chem. C*. 115 (2011) 1220–1230. doi:10.1021/jp106538z.
- 25 [49] O.R. Inderwildi, S.J. Jenkins, D.A. King, Mechanistic studies of hydrocarbon combustion and synthesis on noble metals, *Angew. Chemie*
26 *- Int. Ed.* 47 (2008) 5253–5255. doi:10.1002/anie.200800685.
- 27 [50] S. Eckle, H.G. Anfang, R.J. Behm, Reaction Intermediates and Side Products in the Methanation of CO and CO₂ over Supported Ru
28 Catalysts in H₂-Rich Reformate Gases, *J. Phys. Chem. C*. 115 (2011) 1361–1367. doi:10.1021/jp108106t.
- 29 [51] E. Zağlı, J.L. Falconer, Carbon dioxide adsorption and methanation on ruthenium, *J. Catal.* 69 (1981) 1–8. doi:10.1016/0021-
30 9517(81)90122-6.
- 31 [52] G.D. Weatherbee, C.H. Bartholomew, Hydrogenation of CO₂ on Group VIII Metals II. Kinetics and Mechanism of CO₂ hydrogenation
32 on Nickel, *J. Catal.* 77 (1982) 460–472.
- 33 [53] N.M. Gupta, V.S. Kamble, R.M. Iyer, K. Ravindranathan Thampi, M. Grätzel, The Transient Species Formed over Ru-RuO_x/TiO₂
34 Catalyst in the CO and CO + H₂ Interaction : FTIR Spectroscopic Study, *J. Catal.* 137 (1992) 473–486.
- 35 [54] M. Marwood, R. Doepper, A. Renken, In-situ surface and gas phase analysis for kinetic studies under transient conditions The catalytic
36 hydrogenation of CO₂, *Appl. Catal. A Gen.* 151 (1997) 223–246. doi:10.1016/S0926-860X(96)00267-0.
- 37 [55] X. Wang, Y. Hong, H. Shi, J. Szanyi, Kinetic modeling and transient DRIFTS-MS studies of CO₂ methanation over Ru/Al₂O₃ catalysts,
38 *J. Catal.* 343 (2016) 185–195. doi:10.1016/j.jcat.2016.02.001.
- 39 [56] Y. Traa, J. Weitkamp, Kinetics of the Methanation of Carbon Dioxide over Ruthenium on Titania, *Chem. Eng. Technol.* 21 (1999) 291–
40 293.
- 41 [57] J. Sirita, S. Phanichphant, F.C. Meunier, Quantitative analysis of adsorbate concentrations by diffuse reflectance FT-IR, *Anal. Chem.* 79
42 (2007) 3912–3918. doi:10.1021/ac0702802.
- 43 [58] H. Li, M. Rivallan, F. Thibault-Starzyk, A. Travert, F.C. Meunier, Effective bulk and surface temperatures of the catalyst bed of FT-IR
44 cells used for in situ and operando studies., *Phys. Chem. Chem. Phys.* 15 (2013) 7321–7327. doi:10.1039/c3cp50442e.
- 45 [59] G.H. Yokomizo, A.T. Bell, Isotopic tracer and NMR studies of carbonaceous species present during CO hydrogenation over Ru TiO₂, *J.*
46 *Catal.* 119 (1989) 467–482. doi:10.1016/0021-9517(89)90175-9.
- 47 [60] K.R. Krishna, A.T. Bell, An Isotopic Tracer Study of the Deactivation of Ru/TiO₂ Catalysts during Fischer-Tropsch Synthesis, 130 (1991)

- 1 597–610.
- 2 [61] N.M. Gupta, V.P. Londhe, V.S. Kamble, Gas-Uptake, Methanation, and Microcalorimetric Measurements on the Coadsorption of CO
3 and H₂ over Polycrystalline Ru and a Ru/TiO₂ Catalyst, *J. Catal.* 169 (1997) 423–437.
- 4 [62] J. Szanyi, J.H. Kwak, Dissecting the steps of CO₂ reduction: 1. The interaction of CO and CO₂ with γ -Al₂O₃: an in situ FTIR study., *Phys.*
5 *Chem. Chem. Phys.* 16 (2014) 15117–15125. doi:10.1039/c4cp00616j.
- 6 [63] T. Montanari, L. Castoldi, L. Lietti, G. Busca, Basic catalysis and catalysis assisted by basicity: FT-IR and TPD characterization of
7 potassium-doped alumina, *Appl. Catal. A Gen.* 400 (2011) 61–69. doi:10.1016/j.apcata.2011.04.016.
- 8 [64] C. Morterra, A. Zecchina, S. Coluccia, I.r. Spectroscopic Study of CO₂ adsorption onto η -Al₂O₃, *J. Chem. Soc., Faraday Trans. 1.* 73
9 (1977) 1544–1560. doi:10.1039/F19777301544.
- 10 [65] C. Morterra, G. Magnacca, A case study: surface chemistry and surface structure of catalytic aluminas, as studied by vibrational
11 spectroscopy of adsorbed species, *Catal. Today.* 27 (1996) 497–532. doi:10.1016/0920-5861(95)00163-8.
- 12 [66] G. Busca, J. Lamotte, J. Lavalley, V. Lorenzelli, FT-IR study of the adsorption and transformation of formaldehyde on oxide surfaces, *J.*
13 *Am. Chem. Soc.* 109 (1987) 5197–5202. doi:10.1021/ja00251a025.
- 14 [67] R.A. Dalla Betta, Carbon monoxide adsorption on supported ruthenium, *J. Phys. Chem.* 79 (1975) 2519–2525. doi:10.1021/j100590a015.
- 15 [68] N.M. Gupta, V.S. Kamble, V.B. Kartha, R.M. Iyer, K. Ravindranathan Thampi, M. Grätzel, FTIR Spectroscopic Study of the Interaction
16 of CO₂ and CO₂+H₂ over Partially Oxidized Ru/TiO₂ Catalyst, *J. Catal.* 146 (1994) 173–184. doi:https://doi.org/10.1016/0021-
17 9517(94)90020-5.
- 18 [69] S.Y. Chin, C.T. Williams, M.D. Amiridis, FTIR studies of CO adsorption on Al₂O₃- and SiO₂-supported Ru catalysts, *J. Phys. Chem. B.*
19 110 (2006) 871–882. doi:10.1021/jp053908q.
- 20 [70] D. Lorito, A. Paredes-Nunez, C. Mirodatos, Y. Schuurman, F.C. Meunier, Determination of formate decomposition rates and relation to
21 product formation during CO hydrogenation over supported cobalt, *Catal. Today.* 259 (2015) 192–196. doi:10.1016/j.cattod.2015.06.027.
- 22 [71] J. Datka, Z. Sarbak, R.P. Eischens, Infrared Study of Coke on Alumina and Zeolite, *J. Catal.* 145 (1994) 544–550.
23 doi:10.1006/jcat.1994.1065.
- 24 [72] Z. Sarbak, Fourier-Transform Infrared studies on Coke formation over Alumina Silica-Alumina and Zeolites, *React. Kinet. Catal. Lett.*
25 69 (2000) 177–181.
- 26 [73] A. de Klerk, Fischer-Tropsch Synthesis, in: *Fischer-Tropsch Refin.*, Wiley-VCH Verlag GmbH & Co. KGaA, Weinheim, Germany,
27 2011: pp. 73–103. doi:10.1002/9783527635603.ch4.
- 28 [74] A.R. Garcia, J.L. da Silva, L.M. Ilharco, Chemical adsorption of acetic acid and deuterated acetic acid on Ru(0001), by RAIRS, *Surf.*
29 *Sci.* 415 (1998) 183–193. doi:10.1016/S0039-6028(98)00590-1.
- 30 [75] P. Panagiotopoulou, D.I. Kondarides, X.E. Verykios, Mechanistic aspects of the selective methanation of CO over Ru/TiO₂ catalyst,
31 *Catal. Today.* 181 (2012) 138–147. doi:10.1016/j.cattod.2011.05.030.
- 32 [76] H. Yamasaki, Y. Kobori, S. Naito, T. Onishi, K. Tamaru, Infrared Study of the Reaction of H₂+CO on a Ru/SiO₂ Catalyst, *J. Chem. Soc.*
33 *Faraday Trans. 1 Phys. Chem. Condens. Phases.* 77 (1981) 2913–2925. doi:10.1039/F19817702913.
- 34 [77] A. Paredes-Nunez, D. Lorito, N. Guilhaume, C. Mirodatos, Y. Schuurman, F.C. Meunier, Nature and reactivity of the surface species
35 observed over a supported cobalt catalyst under CO/H₂ mixtures, *Catal. Today.* 242 (2015) 178–183. doi:10.1016/j.cattod.2014.04.033.
- 36